

Mass Ratio of Binary Black Holes Determined from LIGO/Virgo Data Restricted to Small False Alarm Rate

Tomoya Kinugawa^{(1)*}, Takashi Nakamura⁽²⁾, and Hiroyuki Nakano⁽³⁾

¹*Faculty of Engineering, Shinshu University, Nagano, 380-8553, Japan*

²*Department of Physics, Graduate School of Science, Kyoto University, Kyoto 606-8502, Japan*

³*Faculty of Law, Ryukoku University, Kyoto 612-8577, Japan*

27 July 2023

ABSTRACT

Binary black-hole mergers up to the third observing run with the minimum false alarm rate smaller than 10^{-5} yr^{-1} tell us that the mass ratio of two black holes follows $m_2/m_1 = 0.723$ with the chance probability of 0.00301% for $M_{\text{chirp}} > 18M_{\odot}$ where $M_{\text{chirp}} (= (m_1 m_2)^{3/5} / (m_1 + m_2)^{1/5})$ is called the chirp mass of binary with masses m_1 and $m_2 (< m_1)$. We show that the relation of $m_2/m_1 = 0.723$ is consistent if the binaries consist of population III stars which are the first stars in the universe. On the other hand, it is found for $M_{\text{chirp}} < 18M_{\odot}$ that the mass ratio follows $m_2/m_1 = 0.601$ with the chance probability of 0.117% if we ignore GW190412 with $m_2/m_1 \sim 0.32$. This suggests the different origin from that for $M_{\text{chirp}} > 18M_{\odot}$.

Key words: stars: population III, binaries: general relativity, gravitational waves, black hole mergers

1 INTRODUCTION AND DATA WITH SMALL FALSE ALARM RATE

Possible origin of massive binary black holes (BBHs) with total mass $\sim 65M_{\odot}$ like GW150914 which is the world’s first observation of gravitational waves (GWs), is Population (Pop) III stars. Theoretically, GW events like GW150914 were predicted by Kinugawa et al. (2014) before the discovery of GW150914 by Abbott et al. (2016). After that, various compact object binaries have been observed by LIGO/Virgo GW detectors.

Many of them are BBHs (see, e.g., the third Gravitational-wave Transient Catalog (GWTC-3) of The LIGO Scientific Collaboration et al. (2021)). The GW events with $\text{FAR}_{\text{min}} < 1 \times 10^{-5} \text{ yr}^{-1}$ in Abbott et al. (2023) are summarized in Table 1¹. Here, FAR_{min} means the minimum false alarm rate (FAR) evaluated by various pipelines used in the GW data analysis. The reason for this restriction of events having the low value of FAR is to treat more accurate tendency of the events. In Table 1, we show the event name, primary mass m_1 , secondary mass m_2 , chirp mass M_{chirp}

$$M_{\text{chirp}} = \frac{(m_1 m_2)^{3/5}}{(m_1 + m_2)^{1/5}}, \quad (1)$$

luminosity distance D_L , and mass ratio q

$$q = \frac{m_2}{m_1}. \quad (2)$$

* E-mail: kinugawa@shinshu-u.ac.jp

¹ We should note that because there are some updates during this work, we use the latest ones from the online GWTC (The LIGO Scientific Collaboration et al. 2023).

BNS, NS-BH, MGCO-BH, and BBH in the column of “Binary type” mean binary neutron star, neutron star-black hole binary, mass-gap compact object²-black hole binary, and binary black hole, respectively.

In Abbott et al. (2023), the events with $\text{FAR}_{\text{min}} < 1 \text{ yr}^{-1}$ were used for BBHs, and the merger rate ($16\text{--}130 \text{ yr}^{-1} \text{ Gpc}^{-3}$), substructure in the chirp mass distribution (peak around $8M_{\odot}$, weak structure around $15M_{\odot}$, and peak around $30M_{\odot}$), population model to explain the observation etc. were studied. As for the mass ratio distribution, a power law was treated to model it (see, e.g., Mandel & Broekgaarden (2022) for rates of compact object coalescences, and references therein).

In the following, we focus only on BBHs, and especially the masses³. Although the mass ratio of binaries is estimated less accurately than the chirp mass, we can find several studies on the mass ratio related to Abbott et al. (2023). Tiwari (2022) showed that there is no prominent dependence either on the chirp mass or the aligned spin in the mass ratio distribution from the 69 GW events with $\text{FAR}_{\text{min}} < 1 \text{ yr}^{-1}$. Here, it should be noted that the estimation of spins is more difficult than the mass ratio. In our galaxy, Wagg et al.

² The mass of MGCOs lies in $2\text{--}5M_{\odot}$. See Kinugawa et al. (2021b) for details.

³ There are also studies on the spins, for example, see Fishbach et al. (2022) for limits on hierarchical BH mergers from an effective inspiral spin parameter. To extract more detailed information of spins, we will require multiband GW observations (Isoyama et al. 2018) with a decihertz GW detector, B-DECIGO (Nakamura et al. 2016).

Table 1. Event name (the YYMMDD_hhmmss format), primary mass m_1 , secondary mass m_2 , chirp mass M_{chirp} in unit of the solar mass, M_{\odot} , and luminosity distance D_L [Mpc] from [The LIGO Scientific Collaboration et al. \(2023\)](#). These are expressed by the median and 90%-symmetric credible interval. The mass ratio q is evaluated by using the median values of m_1 and m_2 . Binary type shows binary neutron star (BNS), neutron star-black hole binary (NS-BH), mass-gap compact object-black hole binary (MGCO-BH), or binary black hole (BBH). Here, we focus only on events with $\text{FAR}_{\text{min}} < 1 \times 10^{-5} \text{ yr}^{-1}$ where FAR_{min} means the minimum FAR evaluated by various GW data analyses. These events have the probability of astrophysical (signal) origin, $p_{\text{astro}} > 0.99$. The data are sorted by M_{chirp} . The first 2 events are BNSs and NS-BH binaries. The next 14 events are BBHs and a MGCO-BH, and have $M_{\text{chirp}} < 18 M_{\odot}$, and the final 20 events are BBHs and have $M_{\text{chirp}} > 18 M_{\odot}$.

Event name	m_1	m_2	M_{chirp}	D_L	q	Binary type
GW170817	$1.46^{+0.12}_{-0.1}$	$1.27^{+0.09}_{-0.09}$	$1.186^{+0.001}_{-0.001}$	40^{+7}_{-15}	0.87	BNS
GW200115_042309	$5.9^{+2.5}_{-2.5}$	$1.44^{+0.85}_{-0.29}$	$2.43^{+0.05}_{-0.07}$	290^{+150}_{-100}	0.24	NS-BH
GW190924_021846	$8.8^{+4.3}_{-1.8}$	$5.1^{+1.2}_{-1.5}$	$5.8^{+0.2}_{-0.2}$	550^{+220}_{-220}	0.58	BBH
GW190814_211039	$23.3^{+1.4}_{-1.4}$	$2.6^{+0.1}_{-0.1}$	$6.11^{+0.06}_{-0.05}$	230^{+40}_{-50}	0.11	MGCO-BH
GW191129_134029	$10.7^{+4.1}_{-2.1}$	$6.7^{+1.5}_{-1.7}$	$7.31^{+0.43}_{-0.28}$	790^{+260}_{-330}	0.63	BBH
GW200202_154313	$10.1^{+3.5}_{-1.4}$	$7.3^{+1.1}_{-1.7}$	$7.49^{+0.24}_{-0.2}$	410^{+150}_{-160}	0.72	BBH
GW170608	$11^{+5.5}_{-1.7}$	$7.6^{+1.4}_{-2.2}$	$7.9^{+0.2}_{-0.2}$	320^{+120}_{-110}	0.69	BBH
GW191216_213338	$12.1^{+4.6}_{-2.3}$	$7.7^{+1.6}_{-1.9}$	$8.33^{+0.22}_{-0.19}$	340^{+120}_{-130}	0.64	BBH
GW190707_093326	$12.1^{+2.6}_{-2}$	$7.9^{+1.6}_{-1.3}$	$8.4^{+0.6}_{-0.4}$	850^{+340}_{-400}	0.65	BBH
GW191204_171526	$11.9^{+3.3}_{-1.8}$	$8.2^{+1.4}_{-1.6}$	$8.55^{+0.38}_{-0.27}$	650^{+190}_{-250}	0.69	BBH
GW190728_064510	$12.5^{+6.9}_{-2.3}$	$8^{+1.7}_{-2.6}$	$8.6^{+0.6}_{-0.3}$	880^{+260}_{-380}	0.64	BBH
GW200316_215756	$13.1^{+10.2}_{-2.9}$	$7.8^{+1.9}_{-2.9}$	$8.75^{+0.62}_{-0.55}$	1120^{+470}_{-440}	0.60	BBH
GW151226	$13.7^{+8.8}_{-3.2}$	$7.7^{+2.2}_{-2.5}$	$8.9^{+0.3}_{-0.3}$	450^{+180}_{-190}	0.56	BBH
GW190720_000836	$14.2^{+5.6}_{-3.3}$	$7.5^{+2.2}_{-1.8}$	$9^{+0.4}_{-0.8}$	770^{+650}_{-260}	0.53	BBH
GW190412_053044	27.7^{+6}_{-6}	$9^{+2}_{-1.4}$	$13.3^{+0.5}_{-0.5}$	720^{+240}_{-220}	0.32	BBH
GW190512_180714	$23.2^{+5.6}_{-5.6}$	$12.5^{+3.5}_{-2.6}$	$14.6^{+1.4}_{-0.9}$	1460^{+510}_{-590}	0.54	BBH
GW191215_223052	$24.9^{+7.1}_{-4.1}$	$18.1^{+3.8}_{-4.1}$	$18.4^{+2.2}_{-1.7}$	1930^{+890}_{-860}	0.73	BBH
GW190408_181802	$24.8^{+5.4}_{-3.5}$	$18.5^{+3.3}_{-4}$	$18.5^{+1.9}_{-1.2}$	1540^{+440}_{-620}	0.75	BBH
GW170104	$30.8^{+7.3}_{-5.6}$	$20^{+4.9}_{-4.6}$	$21.4^{+2.2}_{-1.8}$	990^{+440}_{-430}	0.65	BBH
GW170814	$30.6^{+5.6}_{-3}$	$25.2^{+2.8}_{-4}$	$24.1^{+1.4}_{-1.1}$	600^{+150}_{-220}	0.82	BBH
GW190915_235702	$32.6^{+8.8}_{-4.9}$	$24.5^{+4.9}_{-5.8}$	$24.4^{+3}_{-2.3}$	1750^{+710}_{-650}	0.75	BBH
GW190828_063405	$31.9^{+5.4}_{-4.1}$	$25.8^{+4.9}_{-5.3}$	$24.6^{+3.6}_{-2}$	2070^{+650}_{-920}	0.81	BBH
GW170809	$35^{+8.3}_{-5.9}$	$23.8^{+5.1}_{-5.2}$	$24.9^{+2.1}_{-1.7}$	1030^{+320}_{-390}	0.68	BBH
GW190630_185205	$35.1^{+6.5}_{-5.5}$	$24^{+5.5}_{-5.2}$	$25.1^{+2.2}_{-2.1}$	870^{+530}_{-360}	0.68	BBH
GW200311_115853	$34.2^{+6.4}_{-3.8}$	$27.7^{+4.1}_{-5.9}$	$26.6^{+2.4}_{-2}$	1170^{+280}_{-400}	0.81	BBH
GW200129_065458	$34.5^{+9.9}_{-3.2}$	$28.9^{+3.4}_{-9.3}$	$27.2^{+2.1}_{-2.3}$	900^{+290}_{-380}	0.84	BBH
GW200112_155838	$35.6^{+6.7}_{-4.5}$	$28.3^{+4.4}_{-5.9}$	$27.4^{+2.6}_{-2.1}$	1250^{+430}_{-460}	0.79	BBH
GW150914	$35.6^{+4.7}_{-3.1}$	$30.6^{+3}_{-4.4}$	$28.6^{+1.7}_{-1.5}$	440^{+150}_{-170}	0.86	BBH
GW170823	$39.5^{+11.2}_{-6.7}$	$29^{+6.7}_{-7.8}$	$29.2^{+4.6}_{-3.6}$	1940^{+970}_{-900}	0.73	BBH
GW190503_185404	$41.3^{+10.3}_{-7.7}$	$28.3^{+7.5}_{-9.2}$	$29.3^{+4.5}_{-4.4}$	1520^{+630}_{-600}	0.69	BBH
GW190727_060333	$38.9^{+8.9}_{-6}$	$30.2^{+6.5}_{-8.3}$	$29.4^{+4.6}_{-3.7}$	3070^{+1300}_{-1230}	0.78	BBH
GW200224_222234	$40^{+6.9}_{-4.5}$	$32.5^{+5}_{-7.2}$	$31.1^{+3.2}_{-2.6}$	1710^{+490}_{-640}	0.81	BBH
GW190521_074359	$43.4^{+5.8}_{-5.5}$	$33.4^{+5.2}_{-6.8}$	$32.8^{+3.2}_{-2.8}$	1080^{+580}_{-530}	0.77	BBH
GW191222_033537	$45.1^{+10.9}_{-8}$	$34.7^{+9.3}_{-10.5}$	$33.8^{+7.1}_{-5}$	3000^{+1700}_{-1700}	0.77	BBH
GW190519_153544	$65.1^{+10.8}_{-11}$	$40.8^{+11.5}_{-12.7}$	$44.3^{+6.8}_{-7.5}$	2600^{+1720}_{-960}	0.63	BBH
GW190602_175927	$71.8^{+18.1}_{-14.6}$	$44.8^{+15.5}_{-19.6}$	$48^{+9.5}_{-9.7}$	2840^{+1930}_{-1280}	0.62	BBH

(2022) give a prediction of the mass ratio distribution with a peak at $q \approx 0.4$ for BBHs observed by a 4 yr LISA observation ([Amaro-Seoane et al. 2017](#)) in their fiducial model. In simulations for hierarchical triples from low-mass young star clusters, [Trani et al. \(2022\)](#) found $q \approx 0.3$ which is lower than that from binaries (see, e.g., [Rastello et al. \(2021\)](#)). [Broekgaarden et al. \(2022a\)](#) showed that at least 95% of BBH mergers detectable by LIGO/Virgo/KAGRA (LVK) detec-

tor network at design sensitivity have $q \gtrsim 0.25$ in their 560 models. [Stegmann et al. \(2022b\)](#) presented orbital properties (masses, mass ratio, eccentricity, orbital separation etc.) of surviving systems after a BBH has formed in the inner binary and those of BBHs which are formed from an isolated binary population for metallicities, $Z = 0.01 Z_{\odot}$ and Z_{\odot} , where Z_{\odot} is the solar metallicity, obtained by using a new triple stellar evolution code. Using the 69 GW events with

$\text{FAR}_{\min} < 1 \text{ yr}^{-1}$, Li et al. (2022) found that the observed BBHs have a much stronger preference for equal mass binaries in their parameterized primary-mass distributions. Using direct N -body simulations for star cluster models, Chattopadhyay et al. (2022) found that the distributions of the mass ratio have median values in the range of 0.8–0.9 (except for one model). Mould et al. (2022a) have prepared a deep-learning pipeline to constrain properties of hierarchical black-hole mergers. In the field of galaxies, Stegmann et al. (2022a) discussed BBHs starting from hierarchical triple population and isolated binary population, and found that the observed lower mass ratio ($q \lesssim 0.5$) BBHs can be explained by the contribution from the outer binary channel of the triple population. In mass-ratio reversal systems where the second BH to form in the binary are more massive than the first BH, Broekgaarden et al. (2022b) found that BBHs with $M_{\text{chirp}} \gtrsim 10 M_{\odot}$ and $q \gtrsim 0.6$ are dominant in the GW observation (see also Mould et al. (2022b)). Briel et al. (2023) introduced super-Eddington accretion into a population synthesis code. Antonini et al. (2023) discussed a scenario of merging BBHs which are formed dynamically in globular clusters, and found that the observed events shown in GWTC-3 cannot be explained in the above scenario (see also Mahapatra et al. (2022)). In Franciolini et al. (2022); Escrivà et al. (2023), the mass ratio has been discussed by treating a varying equation of state at the QCD epoch in primordial BH formation scenario (see also Carr et al. (2023) for a recent review on primordial BHs). Edelman et al. (2023) have suggested some possible plateaus at several mass ratios in the distribution by using a data-driven, non-parametric model. Oh et al. (2023) have discussed merging compact binaries with highly asymmetric mass ratios. Costa et al. (2023) discussed BBHs from Pop II ($Z = 10^{-4}$) and III ($Z = 10^{-11}$) stars in their models, and found that the mass ratios for Pop II BBHs are almost $q \sim 1$ and the peak of mass ratios for Pop III BBHs is $q = 0.8 - 0.9$ in most of their models. In Santoliquido et al. (2023), the redshift dependence of mass ratio of Pop III BBHs was presented. In their models, Pop III BBHs merging at low redshift ($z \lesssim 4$) have low mass ratios, $q \approx 0.5 - 0.7$ (the median values), while typically $q \sim 0.9$ at high redshift. For star clusters, Arca Sedda et al. (2023b) have investigated various types of compact binary mergers by using their database (Arca Sedda et al. 2023a).

2 ANALYSIS

In our previous study (Kinugawa et al. 2021a), we found a very simple relation, $m_2 \simeq 0.7 m_1$ ⁴, for BBHs with $M_{\text{chirp}} \gtrsim 20 M_{\odot}$ summarized in GWTC-2 (Abbott et al. 2021), and that this relation is consistent with the mass distribution in our population synthesis simulations of Pop III stars.

Therefore, first, we focus only on 20 BBH events with $M_{\text{chirp}} > 18 M_{\odot}$ instead of $M_{\text{chirp}} > 20 M_{\odot}$ given in Table 1. This is because there exists a small gap in the chirp mass between GW190512_180714 and GW191215_223052. Figure 1 shows m_1 and m_2 of these events. Assuming $m_2 = 0$

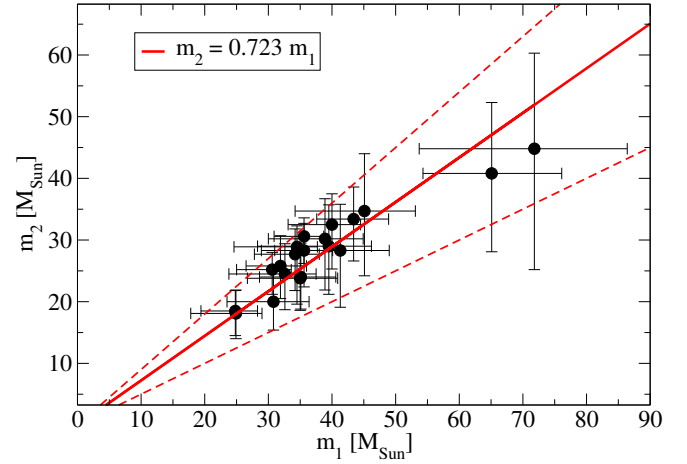


Figure 1. 20 BBH events with $M_{\text{chirp}} > 18 M_{\odot}$ in Table 1. We present the median and 90%-symmetric credible interval for m_1 and m_2 . The fitting (the solid red line) gives $m_2 = 0.723 m_1$, and the correlation coefficient is 0.933 with the chance probability of 0.00301%. As references, we show $m_2 = 0.5 m_1$ and $m_2 = 0.9 m_1$ as the dashed red lines.

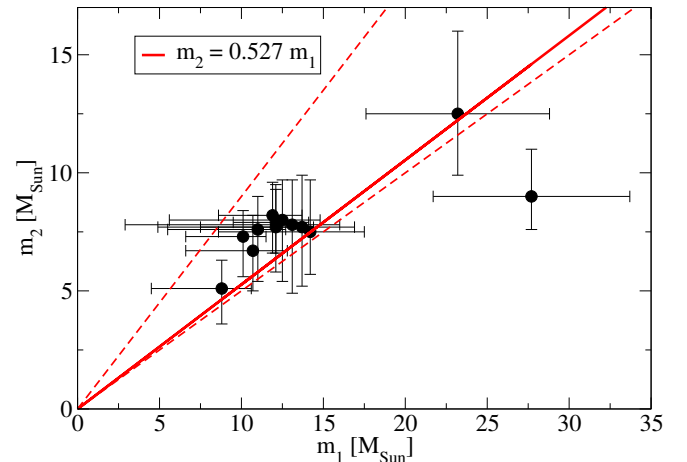


Figure 2. 13 BBH events with $M_{\text{chirp}} < 18 M_{\odot}$ in Table 1. We present the median and 90%-symmetric credible interval for m_1 and m_2 . The fitting (the solid red line) gives $m_2 = 0.527 m_1$, and the correlation coefficient is 0.741. As references, we show $m_2 = 0.5 m_1$ and $m_2 = 0.9 m_1$ as the dashed red lines.

at $m_1 = 0$, the linear fitting function is obtained as

$$m_2 = 0.723 m_1, \quad (3)$$

and the correlation coefficient is 0.933 with the chance probability of 0.00301%.

Next, we treat the remaining BBH events. Figure 2 shows m_1 and m_2 of 13 BBH events with $M_{\text{chirp}} < 18 M_{\odot}$ given in Table 1. Here, we have ignored GW190814_211039 which has a MGCO in the binary. Assuming $m_2 = 0$ at $m_1 = 0$, the linear fitting function is obtained as $m_2 = 0.527 m_1$, and the correlation coefficient is 0.741. The correlation between the data and this fitting function is not so high.

Here, we note that GW190412_053044 has large unequal component masses (Abbott et al. 2020b). As an alternative interpretation of masses for this GW event, we may have

⁴ Broadhurst et al. (2022) also mentioned this relation for nearly all BBH GW events.

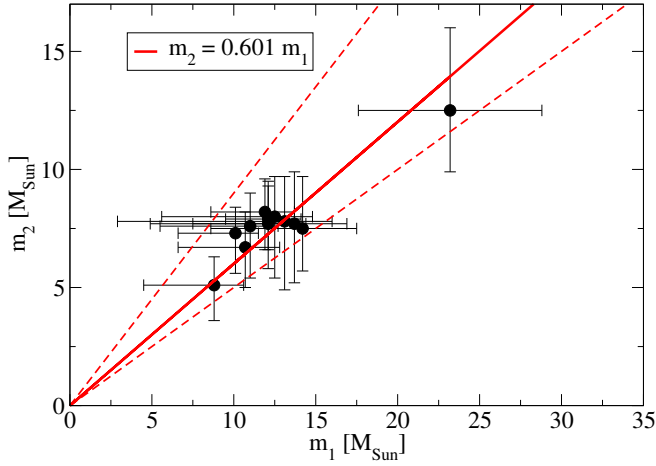


Figure 3. 12 BBH events with $M_{\text{chirp}} < 18 M_{\odot}$ in Table 1. We present the median and 90%-symmetric credible interval for m_1 and m_2 . Here, we have ignored a BBH event, GW190412_053044. The fitting (the solid red line) gives $m_2 = 0.601 m_1$, and the correlation coefficient is 0.937 with the chance probability of 0.117%. As references, we show $m_2 = 0.5 m_1$ and $m_2 = 0.9 m_1$ as the dashed red lines.

$q = 0.31^{+0.05}_{-0.04}$ from a prior with a non-spinning primary and a rapidly spinning secondary (Mandel & Fragos 2020) (see also Kinugawa et al. (2020)). Also, Zevin et al. (2020) found $q \lesssim 0.57$ in the 99% credible level from various models. Interestingly, although the GW data did not prefer Model G with a prior assumption, $\chi_1 = \chi_2 = 0$ in the above paper, this model gave $q \approx 0.55$. Antonelli et al. (2023) have also discussed the most likely formation channel. When we ignore this GW190412_053044 event in the analysis of mass ratio, the fitting is improved as Fig. 3. Assuming $m_2 = 0$ at $m_1 = 0$, the linear fitting function is obtained as

$$m_2 = 0.601 m_1, \quad (4)$$

and the correlation coefficient becomes 0.937 with the chance probability of 0.117%. To argue the origin of BBH events for $M_{\text{chirp}} < 18 M_{\odot}$, we need more examples of BBHs similar to GW190412_053044 in near future by the O4 Observing run (Abbott et al. 2020a).

In Kinugawa et al. (2020), we performed 10^6 Pop III binary evolution by using seven different models with initial conditions of mass function, mass ratio, separation, and eccentricity as well as physical models (see Tables 2 and 3 of Kinugawa et al. (2020) for details of each model). In this paper, we adopt two models called ‘M100’ and ‘K14’. The former model is the one of the best fit model in our previous paper (Kinugawa et al. 2021a). The latter model is the first simulation of the Pop III binary stars performed in 2014 (Kinugawa et al. 2014) as the typical example. The main difference between the two models is the treatment of the mass transfer rate in the stable Roche lobe overflow shown from Eq. (4) to Eq. (7) of Kinugawa et al. (2020) in details.

Figure 4 shows the chirp-mass distribution of 20 BBH events with $M_{\text{chirp}} > 18 M_{\odot}$. The vertical axis shows the expected number of BBHs for a given range of M_{chirp} so that the total number should be 20. The filled (red) circle shows the observed 20 GW events, and the filled square (blue) and diamond (cyan) denote the results of the M100 and K14 mod-

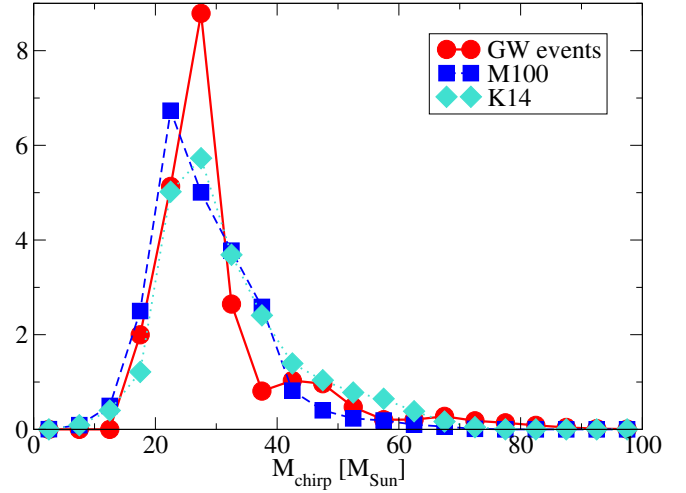


Figure 4. Chirp-mass distribution of 20 BBH events with $M_{\text{chirp}} > 18 M_{\odot}$. The ordinate shows the expected number of BBH for given range of M_{chirp} so that the total number should be 20. The filled (red) circle shows the observed 20 GW events, and the filled square (blue) and diamond (cyan) denote the results of M100 and K14 models by assuming that the total observable number is 20.

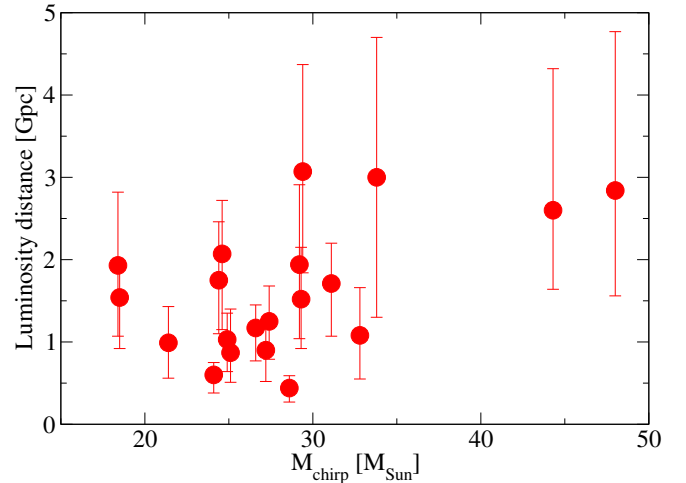


Figure 5. Luminosity distance (D_L) vs. chirp-mass of 20 BBH events with $M_{\text{chirp}} > 18 M_{\odot}$. Here, we present only the median of the chirp mass, and the median and 90%-symmetric credible interval of the luminosity distance.

els by assuming the total observable number is 20. We can see that both the M100 and K14 models fit well with the observed one shown by the red circles.

Figure 5 shows the luminosity distance (D_L) distribution of 20 observed BBH events. We see that $D_L \lesssim 3 \text{ Gpc}$ for $M_{\text{chirp}} \lesssim 30 M_{\odot}$ while $D_L \gtrsim 1.5 \text{ Gpc}$ for $M_{\text{chirp}} \gtrsim 30 M_{\odot}$. But the errors are still large to say the above facts definitely.

3 DISCUSSION

Figures 6 and 7 show the delay time (T_{delay}) distributions for each mass ratio of merging Pop III BBHs in the M100

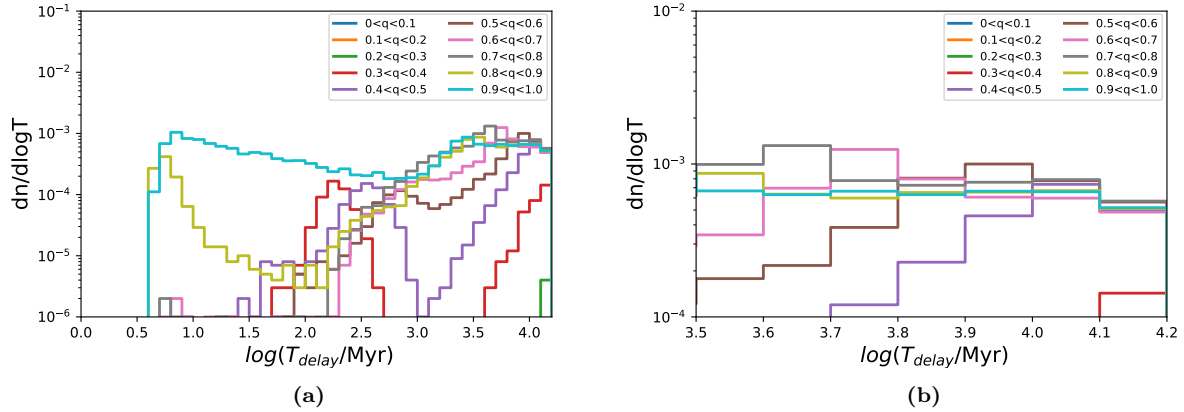


Figure 6. Delay time (T_{delay}) distributions for each mass ratio of merging Pop III BBHs in the M100 model. The distribution is normalized by the number of total Pop III binaries. (a) shows the delay time distributions of BBHs which merge within the Hubble time. (b) shows the delay time distributions of BBHs of which the merger time is more than $10^{3.5}$ Myrs and less than the Hubble time.

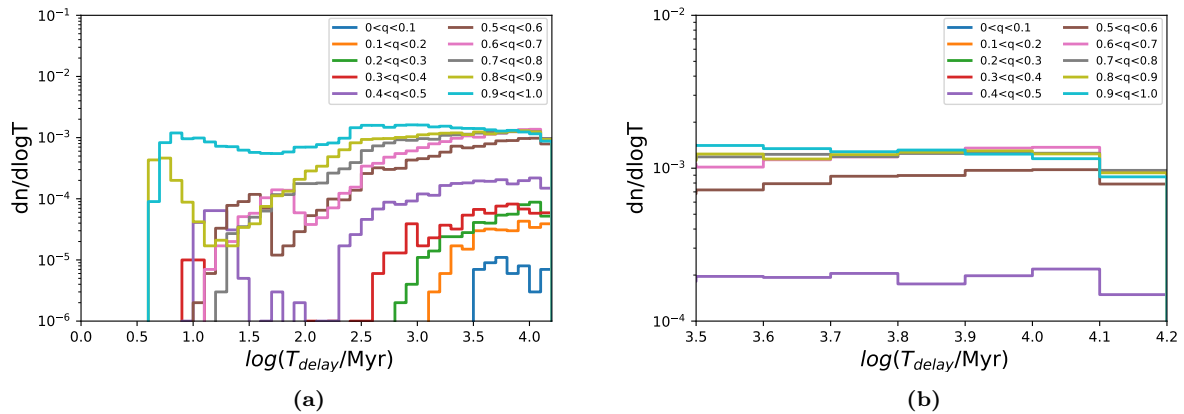


Figure 7. Same figure of Fig. 6 but for the K14 model.

and K14 models, respectively. We present the delay time distributions of Pop III BBHs which merge within the Hubble time in Figs. 6a and 7a, while the delay time distributions of Pop III BBHs of which the merger time is more than $10^{3.5}$ Myrs and less than the Hubble time in Figs. 6b and 7b. These distributions are normalized by the number of total Pop III binaries.

It is found in Figs. 6a and 7a that the nearly equal-mass BBH mergers predominate in a very short delay time region ($T_{\text{delay}} \lesssim 100$ Myrs). In other words, the nearly equal-mass Pop III BBH mergers predominate in the very early universe ($z \gtrsim 10$) since the Pop III stars are born and died at high redshift ($z \gtrsim 10$). These BBH mergers at the high redshift can be observed future GW observatory such as the Einstein telescope (ET) (Hild et al. 2011), the Cosmic Explorer (CE) (Evans et al. 2021), and DECIGO (Seto et al. 2001; Nakamura et al. 2016).

The formation channel is the reason why the equal mass Pop III BBHs merge at the high redshift. In our previous paper (Kinugawa et al. 2020), we classified the Pop III BBH formation channel into the 5 channels such as NoCE, $1CE_P$, $1CE_S$, $1CE_D$, and $2CE$. NoCE means that Pop III BBHs

evolve not via a common envelope phase. $1CE_P$, $1CE_S$, and $1CE_D$ are Pop III BBHs evolved via one common envelope phase caused by the primary giant star, the secondary giant star, or double giant stars, respectively. $2CE$ is the Pop III BBHs experienced more than two common envelope phases. Figure 5 of Kinugawa et al. (2020) shows that almost all Pop III BBHs merging with very short delay time ($T_{\text{delay}} \lesssim 100$ Myrs) evolved via the $1CE_D$ channel.

Figure 8 shows an example of $1CE_D$ channel. Pop III binaries of which initial masses are nearly equal tend to evolve via the $1CE_D$ channel. If the initial masses of a binary are similar, the timescale of evolution is similar as well. Therefore, they both become giant stars at almost the same time and shed their envelopes simultaneously through a double common envelope process. A significant amount of orbital energy is also lost by shedding the outer envelopes of both stars. After that, a very close binary He star tends to remain, and they can become a close BBH which merges within 100 Myrs.

Next, we focus on Figs. 6b and 7b where Pop III BBHs with a long delay time are presented for each mass ratio. Figures 9 and 10 show the mass ratio distributions of merging Pop III BBHs of which delay time is more than $10^{3.5}$ Myrs and less

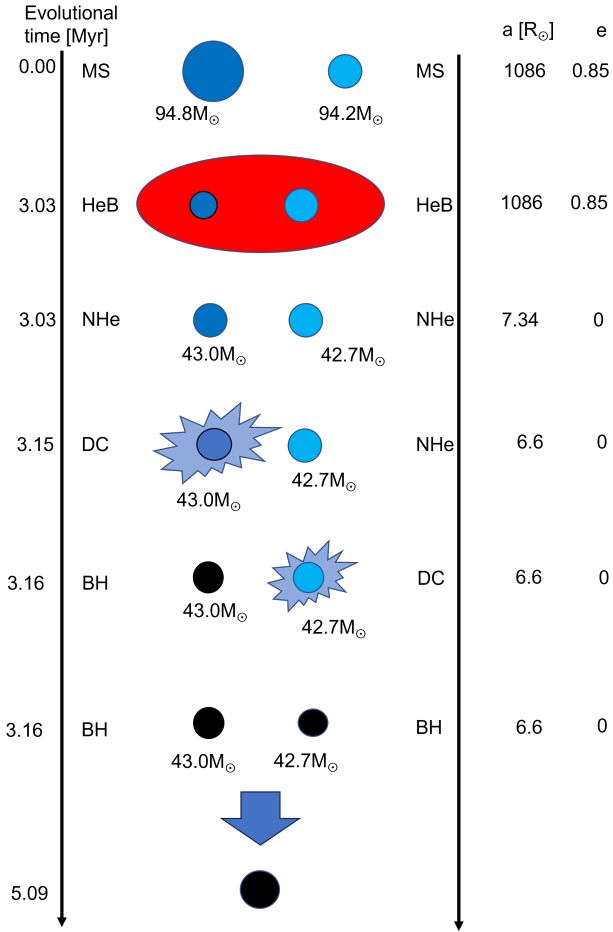


Figure 8. Example of Pop III binary evolution via $1CE_D$ channel. Here, a and e denote the separation and eccentricity, respectively. MS, HeB, NHe, DC and BH mean main-sequence phase, helium-burning phase, naked helium star, degenerate core, and black hole, respectively.

than the Hubble time for M100 and K14 models, respectively. These BBHs can be detected within the detection range of LVK collaboration.

In the M100 model, the main contribution to the mass ratio distribution is the $1CE_P$ channel. Subdominant ones are NoCE and 2CE channels. These channels make BBHs with various mass ratios from 0.4 to 1, unlike the $1CE_D$ channel. In the K14 model, the main contribution is the NoCE channel. Subdominant ones are $1CE_P$ and 2CE channels. This model also has various mass ratio BBH mergers with a long delay time like the M100 model.

According to these results, it is expected that observations at high redshift, unlike observations at low redshift, would exhibit a higher proportion of equal-mass BBH mergers. A comparison between the low-redshift results from the current ground-based GW observations and the high-redshift results from future observations such as ET, CE and DECIGO enables us to check the Pop III origin model.

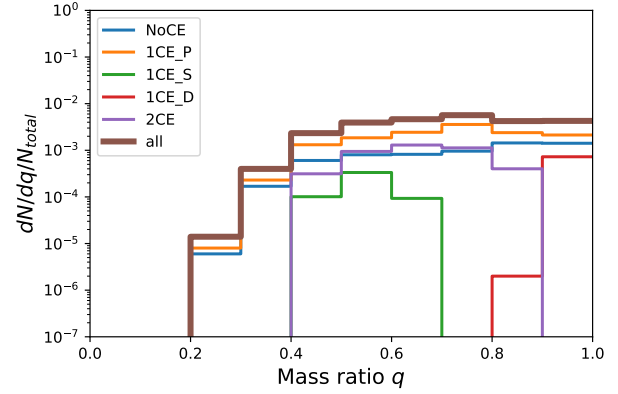


Figure 9. Mass ratio distributions of merging Pop III BBHs of which delay time is more than $10^{3.5}$ Myrs and less than the Hubble time for M100 model.

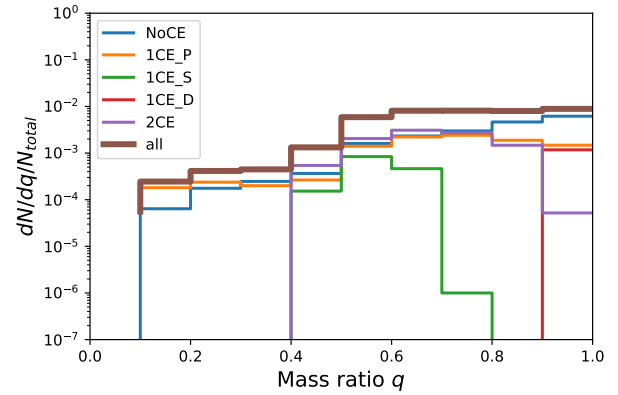


Figure 10. Same figure of Fig. 9 but for the K14 model.

ACKNOWLEDGMENT

T. K. acknowledges support from JSPS KAKENHI Grant Numbers JP21K13915 and JP22K03630. H. N. acknowledges support from JSPS KAKENHI Grant Numbers JP21H01082 and JP21K03582, and also would like to thank to Y. W. for her hospitality.

DATA AVAILABILITY

Results will be shared on reasonable request to the corresponding author.

REFERENCES

- Abbott B. P., et al., 2016, *Physical Review Letters*, **116**, 061102
- Abbott B. P., et al., 2020a, *Living Reviews in Relativity*, **23**, 3
- Abbott R., et al., 2020b, *Phys. Rev. D*, **102**, 043015
- Abbott R., et al., 2021, *Physical Review X*, **11**, 021053
- Abbott R., et al., 2023, *Physical Review X*, **13**, 011048
- Amaro-Seoane P., et al., 2017, arXiv e-prints, p. [arXiv:1702.00786](https://arxiv.org/abs/1702.00786)
- Antonelli A., Kritos K., Ng K. K. Y., Cotesta R., Berti E., 2023, arXiv e-prints, p. [arXiv:2306.11088](https://arxiv.org/abs/2306.11088)

- Antonini F., Gieles M., Dosopoulou F., Chattopadhyay D., 2023, *MNRAS*, **522**, 466
- Arca Sedda M., et al., 2023a, *arXiv e-prints*, p. [arXiv:2307.04805](https://arxiv.org/abs/2307.04805)
- Arca Sedda M., Kamlah A. W. H., Spurzem R., Rizzuto F. P., Giersz M., Naab T., Berczik P., 2023b, *arXiv e-prints*, p. [arXiv:2307.04807](https://arxiv.org/abs/2307.04807)
- Briel M. M., Stevance H. F., Eldridge J. J., 2023, *MNRAS*, **520**, 5724
- Broadhurst T., Diego J. M., Smoot G. F., 2022, *arXiv e-prints*, p. [arXiv:2202.05861](https://arxiv.org/abs/2202.05861)
- Broekgaarden F. S., et al., 2022a, *MNRAS*, **516**, 5737
- Broekgaarden F. S., Stevenson S., Thrane E., 2022b, *ApJ*, **938**, 45
- Carr B., Clesse S., Garcia-Bellido J., Hawkins M., Kuhnel F., 2023, *arXiv e-prints*, p. [arXiv:2306.03903](https://arxiv.org/abs/2306.03903)
- Chattopadhyay D., Hurley J., Stevenson S., Raidani A., 2022, *MNRAS*, **513**, 4527
- Costa G., Mapelli M., Iorio G., Santoliquido F., Escobar G. J., Klessen R. S., Bressan A., 2023, *arXiv e-prints*, p. [arXiv:2303.15511](https://arxiv.org/abs/2303.15511)
- Edelman B., Farr B., Doctor Z., 2023, *ApJ*, **946**, 16
- Escrivà A., Bagui E., Clesse S., 2023, *J. Cosmology Astropart. Phys.*, **2023**, 004
- Evans M., et al., 2021, *arXiv e-prints*, p. [arXiv:2109.09882](https://arxiv.org/abs/2109.09882)
- Fishbach M., Kimball C., Kalogera V., 2022, *ApJ*, **935**, L26
- Franciolini G., Musco I., Pani P., Urbano A., 2022, *Phys. Rev. D*, **106**, 123526
- Hild S., et al., 2011, *Classical and Quantum Gravity*, **28**, 094013
- Isoyama S., Nakano H., Nakamura T., 2018, *PTEP*, **2018**, 073E01
- Kinugawa T., Inayoshi K., Hotokezaka K., Nakauchi D., Nakamura T., 2014, *MNRAS*, **442**, 2963
- Kinugawa T., Nakamura T., Nakano H., 2020, *MNRAS*, **498**, 3946
- Kinugawa T., Nakamura T., Nakano H., 2021a, *MNRAS*, **504**, L28
- Kinugawa T., Nakamura T., Nakano H., 2021b, *Progress of Theoretical and Experimental Physics*, **2021**, 021E01
- Li Y.-J., Wang Y.-Z., Tang S.-P., Yuan Q., Fan Y.-Z., Wei D.-M., 2022, *ApJ*, **933**, L14
- Mahapatra P., Gupta A., Favata M., Arun K. G., Sathyaprakash B. S., 2022, *arXiv e-prints*, p. [arXiv:2209.05766](https://arxiv.org/abs/2209.05766)
- Mandel I., Broekgaarden F. S., 2022, *Living Reviews in Relativity*, **25**, 1
- Mandel I., Fragos T., 2020, *ApJ*, **895**, L28
- Mould M., Gerosa D., Taylor S. R., 2022a, *Phys. Rev. D*, **106**, 103013
- Mould M., Gerosa D., Broekgaarden F. S., Steinle N., 2022b, *MNRAS*, **517**, 2738
- Nakamura T., et al., 2016, *Progress of Theoretical and Experimental Physics*, **2016**, 093E01
- Oh M., Fishbach M., Kimball C., Kalogera V., Ye C., 2023, *arXiv e-prints*, p. [arXiv:2303.06081](https://arxiv.org/abs/2303.06081)
- Rastello S., Mapelli M., Di Carlo U. N., Iorio G., Ballone A., Giacobbo N., Santoliquido F., Tormiamenti S., 2021, *MNRAS*, **507**, 3612
- Santoliquido F., Mapelli M., Iorio G., Costa G., Glover S. C. O., Hartwig T., Klessen R. S., Merli L., 2023, *arXiv e-prints*, p. [arXiv:2303.15515](https://arxiv.org/abs/2303.15515)
- Seto N., Kawamura S., Nakamura T., 2001, *Phys. Rev. Lett.*, **87**, 221103
- Stegmann J., Antonini F., Schneider F. R. N., Tiwari V., Chattopadhyay D., 2022a, *Phys. Rev. D*, **106**, 023014
- Stegmann J., Antonini F., Moe M., 2022b, *MNRAS*, **516**, 1406
- The LIGO Scientific Collaboration et al., 2021, *arXiv e-prints*, p. [arXiv:2111.03606](https://arxiv.org/abs/2111.03606)
- The LIGO Scientific Collaboration The Virgo Collaboration The KAGRA Scientific Collaboration 2023, The Online Gravitational-wave Transient Catalog (GWTC), <https://gwosc.org/eventapi/html/GWTC/>
- Tiwari V., 2022, *ApJ*, **928**, 155
- Trani A. A., Rastello S., Di Carlo U. N., Santoliquido F., Tanikawa A., Mapelli M., 2022, *MNRAS*, **511**, 1362
- Wagg T., Broekgaarden F. S., de Mink S. E., Frankel N., van Son L. A. C., Justham S., 2022, *ApJ*, **937**, 118
- Zevin M., Berry C. P. L., Coughlin S., Chatziioannou K., Vitale S., 2020, *ApJ*, **899**, L17